Fat Segmentation on Chest CT images via fuzzy models

Yubing Tong[1], Jayaram K. Udupa[1], Caiyun Wu[1], Gargi Pednekar[1], Janani Rajan Subramanian[1], David J Lederer[3], Jason Christie[2], Drew A. Torigian[1]
[1]Medical Image Processing Group, Department of Radiology, University of Pennsylvania, Philadelphia, PA 19104; [2]Division of Pulmonary and Critical Care Medicine, Hospital of the University of Pennsylvania Center for Clinical Epidemiology and Biostatistics, University of Pennsylvania School of Medicine, Philadelphia, PA 19104; [3]Pulmonary & Intensive Care Translational Outcomes Research Group, Division of Pulmonary, Allergy, and Critical Care Medicine, Columbia University Medical Center, NY, 10032.

ABSTRACT

Quantification of fat throughout the body is vital for the study of many diseases. In the thorax, it is important for lung transplant candidates since obesity and being underweight are contraindications to lung transplantation given their associations with increased mortality. Common approaches for thoracic fat segmentation are all interactive in nature, requiring significant manual effort to draw the interfaces between fat and muscle with low efficiency and questionable repeatability. The goal of this paper is to explore a practical way for the segmentation of subcutaneous adipose tissue (SAT) and visceral adipose tissue (VAT) components of chest fat based on a recently developed body-wide automatic anatomy recognition (AAR) methodology. The AAR approach involves 3 main steps: building a fuzzy anatomy model of the body region involving all its major representative objects, recognizing objects in any given test image, and delineating the objects. We made several modifications to these steps to develop an effective solution to delineate SAT/VAT components of fat. Two new objects representing interfaces of SAT and VAT regions with other tissues, SatIn and VatIn are defined, rather than using directly the SAT and VAT components as objects for constructing the models. A hierarchical arrangement of these new and other reference objects is built to facilitate their recognition in the hierarchical order. Subsequently, accurate delineations of the SAT/VAT components are derived from these objects. Unenhanced CT images from 40 lung transplant candidates were utilized in experimentally evaluating this new strategy. Mean object location error achieved was about 2 voxels and delineation error in terms of false positive and false negative volume fractions were, respectively, 0.07 and 0.1 for SAT and 0.04 and 0.2 for VAT.

Keywords: Automatic anatomy recognition, fuzzy models, chest fat quantification, image segmentation, CT

1. INTRODUCTION

Quantitative assessment of the properties of fat in the body is important, as certain fat properties including volume, distribution, and composition may be associated with adverse clinical outcomes in various disease settings including obesity, obstructive sleep apnea, cancer, cardiovascular disease, hepatic disease, renal disease, endocrine disorders such as diabetes mellitus, musculoskeletal disease, amongst others, along with adverse outcomes following various surgical procedures such as organ transplantation or tumor resection. In particular, quantitative analysis of thoracic fat, including assessment of the two separate components of fat called subcutaneous adipose tissue (SAT) and visceral adipose tissue (VAT), may be particularly important in certain clinical situations, such as for predicting clinical outcome following lung transplantation or for determining cardiovascular [1-4].

At present, fat assessment in the body is often performed via tomographic imaging either with computed tomography (CT) or magnetic resonance imaging (MRI) [5-7]. However, delineation of the SAT and VAT components of fat is typically performed in an interactive manner, requiring significant manual effort and time, and involving subjective assessment of the boundaries, leading to errors. Thus, there is a dire need for practical methods of recognizing and segmenting the SAT and VAT components of fat automatically to improve the efficiency, reproducibility, and accuracy of quantitative analysis, so that this new information may be utilized for clinical risk stratification and patient prognosis assessment.

Medical Imaging 2016: Image-Guided Procedures, Robotic Interventions, and Modeling,
edited by Robert J. Webster, III, Ziv R. Yaniv, Proc. of SPIE Vol. 9786, 978609
 · doi: 10.1117/12.2217864

Separating the SAT and VAT components is much more difficult in the thorax than in the abdomen [8-10]. There are two main reasons for this. Firstly, it is not obvious how the interface separating these components should be unambiguously defined anatomically in the thorax. In the abdomen, this is quite clear because of the muscle mass separating the two components. Second, and as a consequence of the lack of clearly definable visual boundaries in the image, whatever definition is adopted, it becomes really challenging to devise an automated algorithm to construct meaningful boundaries in the image corresponding to this defined interface where there is no evidence for boundaries in terms of intensity changes in the image. Therefore, notwithstanding the lack of a standard definition of the two components, manual delineation is commonly used for this task of separated segmentation of SAT and VAT in the chest [11]. We note, however, that more automated techniques have been developed for delineating pockets of fat in the chest, such as pericardial fat [12, 13], when there is a clear visually discernible and hence definable boundary.

In this paper, we describe an automated method and some early results for the problem of SAT/VAT separated segmentation on chest CT images. The method adapts to this application a recently developed technology called automatic anatomy recognition (AAR) [14, 15] which aims to recognize and delineate automatically numerous internal solid organs body-wide on CT, MRI, and positron emission tomography (PET) images based on population fuzzy anatomy models.

2. MATERIALS & METHODS

Image Data

This retrospective study was conducted following approval from the Institutional Review Board at the University of Pennsylvania along with a Health Insurance Portability and Accountability Act waiver. Existing unenhanced CT image data sets from 40 lung transplant candidates, predominantly with idiopathic pulmonary fibrosis (IPF) or chronic obstructive pulmonary disease (COPD), that were previously acquired as part of a separate prospective study at three lung transplant centers (Columbia, Penn, and Duke) were utilized in this study. In these data sets, the image size is 512×512×50-70, with a voxel size of 0.70×0.70-0.97×0.97×5.0 mm^3. The mean age of the patients is 58.0 yrs (± 11.7 yrs) with a mean body mass index (BMI) of 26.4 kg/m^2 (± 4.3). Chest CT scans had been performed per local clinical protocol during full inspiration.

AAR approach for SAT/VAT separation

Given a body region *B*, the AAR approach [10] consists of three steps: building the fuzzy anatomy model *FAM*(*B*) of the body region, recognizing or locating objects of *B* in a given image *I*, and delineating the recognized objects in *I*. The model building step starts with a precise anatomic definition of *B* and all objects in *B* that are considered important for the application at hand. The objects are then precisely delineated on a set of images designated for creating the model, and the anatomy model of *B* is built using the delineations. *FAM*(*B*) is subsequently utilized to localize objects and delineate them in any given image *I*.

Object definition

Objects considered in this study are selected from the viewpoint of making AAR effective in the task of SAT/VAT separation. They include: the outer boundary of the skin covering the thoracic body region (TSkin), left pleural space (LPS), right pleural space (RPS), the composite of LPS and RPS denoted LRPS (= LPS + RPS), and two additional objects, denoted VatIn and SatIn, which are super objects containing VAT and SAT components, respectively. The precise definition of these new objects is given below. The thoracic body region is defined as extending from 15 mm superior to the apex of the lungs to 5 mm inferior to the base of the lungs.

We define the thoracic SAT-VAT interface as the interior surface of the rib cage; fat within this surface is considered to be VAT and that external to this surface is defined as SAT for all slices which are superior to the diaphragm. For slices passing through the diaphragm, the definition of SAT remains the same. The VAT component, however, is modified in these slices by removing the visceral fat located within the abdomen. These definitions are illustrated in Figures 1 (a), (b), and (c) for a slice in each of the superior, mid, and inferior portions of the thorax.

(a) (b) (c)

Figure 1. Definition of SAT-VAT interface illustrated through boundary contours drawn on slices: (a) in upper thorax, (b) in mid thorax, and (c) in lower thorax at level of diaphragm.

One possibility is to use exact SAT and VAT 3D regions as objects directly in the AAR approach. Since these regions, especially VAT, have complicated and variable shapes (see Figure 2), we defined the proposed new objects *SatIn* and *VatIn* as follows, which lead to more effective and robust models and subsequently better segmentation. SatIn is a 3D region defined in such a manner that if we apply a threshold corresponding to fat to this region, only and the entirety of the SAT part is captured. VatIn is analogously defined. The binary mask corresponding to the SatIn object is shown in Figure 2a. Figures 2c and 2d show the VatIn mask at different axial slice locations - Figure 2c for a location that cuts through the diaphragm and Figure 2d for a location superior to the dome of the diaphragm. The actual SAT and VAT regions defined by these SatIn and VatIn objects are depicted in Figures 2b, 2e, and 2f.

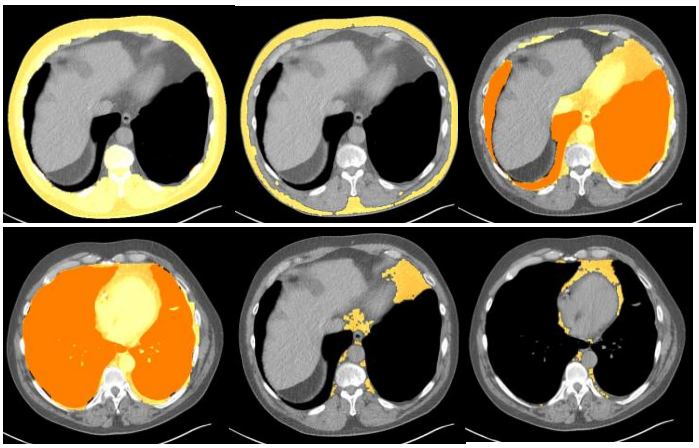

Figure 2. From top to bottom, left to right (a): SatIn. (b): SAT. (c) and (d): VatIn. (e) and (f): VAT.

Building a fuzzy anatomy model

The fuzzy anatomy model of B, $FAM(B)$, consists of five entities: $FAM(B) = (H, M, \rho, \lambda, \eta)$. H here is a hierarchical order (tree) of the objects $O_1,\ldots, O_L$ in B considered for inclusion in the model. Figure 3 shows an example of the hierarchy utilized in this study, where 6 objects in total are included. $M = \{FM_\ell : 1 \le \ell \le L\}$ is a set of fuzzy models, one for each of the L objects. ρ represents parent-to-offspring object relationship in H. $\lambda = \{\lambda_\ell : 1 \le \ell \le L\}$, λ_ℓ being scale factor range of object O_ℓ over the population considered. η is a host of measurements pertaining to objects in B derived from the population.

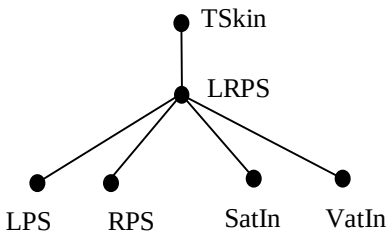

Figure 3. An example of hierarchical structure utilized in this paper.

Object recognition and SAT/VAT delineation

Once *FAM*(*B*) is created, the AAR hierarchical recognition algorithms are applied to any given test image *I*. The recognition algorithms localize an object in *I* by searching for the best pose for placing the fuzzy model of the object in *I*. This is accomplished in two stages. First, through a *one-shot* approach, the pose of the model is determined based on the location of the already recognized parent object and the parent-to-offspring relationship information stored in *FAM*(*B*). This is followed by a refinement of the pose by an optimal object-specific threshold-based search [14].

AAR delineation is performed to determine the exact object extent or boundary in *I*. At the end of the recognition step, we will have determined an optimally pose-adjusted fuzzy model for each object in the chosen hierarchy. Subsequently, the skin object TSkin is delineated in *I* using the AAR delineation algorithms. The reason for the inclusion of other objects, particularly LRPS, LPS, and RPS, is to give a proper recognition context for the main objects of interest, namely SatIn and VatIn. The pose adjusted model *FM*(SatIn) of object SatIn is then further adjusted for its position in *I* by performing a 12-parameter affine registration on *FM*(SatIn) with another image $I_c = I \times FM_t(\text{SatIn})$ where $FM_t(\text{SatIn})$ is a binary image resulting from thresholding *FM*(SatIn) at a low model membership threshold. The result of registration is a new pose adjusted model of SatIn, denoted $FM^p(\text{SatIn})$. The SAT object is finally obtained by thresholding *I* within the fuzzy mask of $FM^p(\text{SatIn})$. The VAT object is subsequently delineated in *I* from knowledge of the delineation of TSkin, SAT, and the pose adjusted model *FM*(VatIn).

3. Results

All objects - Tskin, LPS, RPS, SatIn, and VatIn - were manually segmented in all 40 data sets. This segmented set provides the ground truth for evaluating object recognition and delineation results. We used data sets from 20 subjects for constructing *FAM*(*B*), and the remaining 20 data sets for testing SAT/VAT segmentation. 3D volume renditions of some fuzzy object models generated in this study are displayed in Figure 4 for RPS, LPS, SatIn, and VatIn objects.

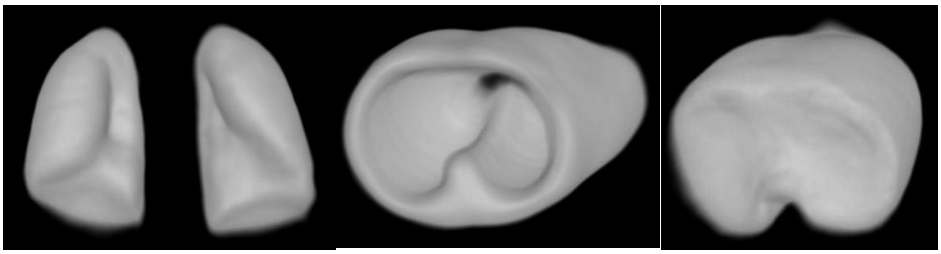

Figure 4. 3D renditions of the fuzzy object models generated for objects (left to right) RPS, LPS, SatIn, and VatIn.

Table 1. AAR Recognition results for TSkin, LRPS, LPS, RPS, SatIn and VatIn.

Object		TSkin	LRPS	LPS	RPS	SatIn	VatIn
Location error (mm)	Mean	6.28	9.34	5.54	6.28	10.99	9.30
	SD	2.09	4.93	2.68	3.75	4.12	4.90
Scale error	Mean	1.02	0.98	0.98	0.99	0.91	0.96
	SD	0.03	0.04	0.04	0.05	0.04	0.04

Quantitative recognition results for the object hierarchy depicted in Figure 3 are summarized in Table 1. Recognition performance is expressed in terms of location and scale errors. Location error (in mm) describes the difference in the location of the pose adjusted model found at the end of the recognition process and the known true location of the object. The scale factor error is expressed as a ratio of the estimated to the actual size of the object. The ideal values for these two error measures are 0 and 1, respectively. Mean location errors for SatIn and VatIn are about 2 voxels, while the scale values are close to 1.

Table 2. Delineation results.

	FNVF		FPVF		HD (mm)	
Objects	Mean	SD	Mean	SD	Mean	SD
SAT	0.10	0.10	0.07	0.03	0.69	0.45
VAT	0.23	0.13	0.04	0.02	4.91	3.01

Table 2 shows quantitative delineation results which are expressed in terms of false negative volume fraction (FNVF), false positive volume fraction (FPVF), and Hausdorff boundary distance (HD). The results are based on the hierarchy shown in Figure 3.

Figure 5 displays sample recognition results for LPS, RPS, SatIn, and VatIn by overlaying the recognition results on the test images. Figure 6 shows sample delineation results for SAT and VAT.

Figure 5. Recognition result examples for RPS, LPS, SatIn, and VatIn.

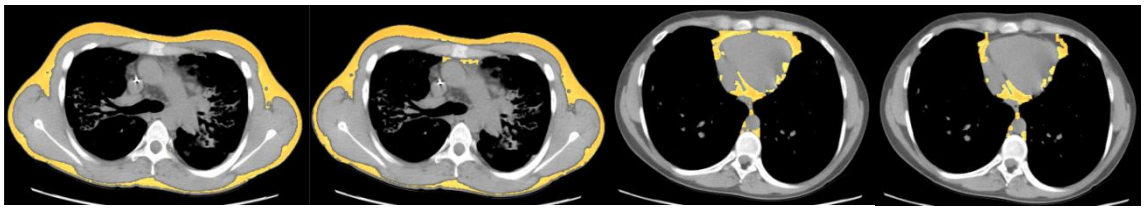

Figure 6. Sample delineation result for SAT (left) and VAT (right), manual segmentation (left) and automatic segmentation (right).

4. CONCLUDING REMARKS

Quantitative analysis of SAT and VAT components via thoracic CT images plays a key role in the study of disease conditions that are affected by the amount, location, and other properties of fat in the body. Automated delineation of these components of adipose tissue in images is the first required step toward those goals. This paper, to our knowledge, is the first attempt to arrive at an automated solution for this difficult problem.

The AAR methodology offers a framework for rapidly prototyping different applications where object localization and delineation are needed. In this paper, we adapted AAR to the problem of separately segmenting the SAT and VAT components of fat in the chest on CT images. The process required carefully identifying the key thoracic objects that are to be considered and their precise definition. In this context, we formulated two new objects (SatIn and VatIn) such that it would become feasible to compute SAT and VAT components by thresholding for fat in these respective objects. We developed their precise anatomic definition and devised algorithms based on AAR to localize them and subsequently to delineate the two fat components.

The proposed approach can segment the SAT component at a level of accuracy which is considered to be high in the segmentation literature. However, the VAT component requires improvement in its false negative component. There is an issue in adequately describing delineation accuracy via FPVF and FNVF when the object of study is sparse (meaning thin or subtle and not blob-like and compact). The VAT fat component in the chest certainly constitutes a sparse object. The issue is that even small delineation errors may lead to large FPVF and FNVF values. When examined visually, our results seem qualitatively quite acceptable and better than the accuracy expressed by FNVF of 20%. Note, however, that the HD value for VAT is quite low, which agrees with our visual impression of accuracy.

Different hierarchical structures for object arrangement can significantly influence AAR recognition, and hence delineation results. There may be other more optimal hierarchies that will yield better delineation for both SAT and VAT. These need to be investigated further.

ACKNOWLEDGEMENT

This research is partly funded by DHHS grants R01 HL114626 (PIs: Christie/Lederer) and R01 HL087115 (Christie).

REFERENCES

[1]Ligibel JA, Alfano CM, Courneya KS, Demark-Wahnefried W, Burger RA, Chlebowski RT, Fabian CJ, Gucalp A, Hershman DL, Hudson MM, Jones LW, Kakarala M, Ness KK, Merrill JK, Wollins DS, Hudis CA., "American Society of Clinical Oncology position statement on obesity and cancer," J Clin Oncol. 1; 32(31):3568-3574 (2014).
[2]Singer JP, Peterson ER, Snyder ME, Katz PP, Golden JA, D'Ovidio F, Bacchetta M, Sonett JR, Kukreja J, Shah L, Robbins H, Van Horn K, Shah RJ, Diamond JM, Wickersham N, Sun L, Hays S, Arcasoy SM, Palmer SM, Ware LB, Christie JD, Lederer, DJ., "Body composition and mortality after adult lung transplantation in the United States," Am J Respir Crit Care Med. 1;190(9):1012-1021 (2014).
[3]Britton KA, Massaro JM, Murabito JM, Kreger BE, Hoffmann U, Fox CS., "Body fat distribution, incident cardiovascular disease, cancer, and all-cause mortality," J Am Coll Cardiol. 62(10):921-925 (2013).
[4]Kyrou I, Randeva HS, Weickert MO, "Clinical Problems Caused by Obesity," In: De Groot LJ, Beck-Peccoz P, Chrousos G, Dungan K, Grossman A, Hershman JM, Koch C, McLachlan R, New M, Rebar R, Singer F, Vinik A, Weickert MO, editors. Endotext. South Dartmouth (MA), (2000). Available from http://www.ncbi.nlm.nih.gov/books/NBK278973/.
[5]Poonawalla, AH, Sjoberg, BP, Rehm, JL, Hernando, D., Hines, CD, Irarrazaval, P., Reeder, SB, "Adipose tissue MRI for quantitative measurement of central obesity," Journal of magnetic resonance imaging: JMRI 37, 707-716 (2013).
[6]Seabolt LA, Welch EB, Silver HJ., "Imaging methods for analyzing body composition in human obesity and cardiometabolic disease," Ann N Y Acad Sci.1353:41-59 (2015).
[7]Fosbøl MØ, Zerahn B., "Contemporary methods of body composition measurement," Clin Physiol Funct Imaging," 35(2):81-97 (2015).
[8]Tong, YB, Udupa, JK, Odhner, D, Sin, S and Arens, R, "Abdominal Adiposity Quantification at MRI via Fuzzy Model–Based Anatomy Recognition," Proceeding of SPIE, Medical Imaging, Vol.8672, 8672R1-7 (2013).
[9]Kyle, UG, Nicod, L., Romand, JA, Slosman, DO, Spiliopoulos, A, and Pichard, C, "Four-year follow-up of body composition in lung transplant patients," Transplantation 75(6): 821-828 (2003).
[10]Najafizadeh, K, Ahmadi, SH, Dezfouli, AA, Mohammadi, F, Kardavani, B, Vishteh, HR, "Fat and bone marrow embolization in a donor as the cause of death in a lung recipient," Transplant Proc. 44, 2924-2926 (2009).
[11]Nakazato, R, Shmilovich, H, Tamarappoo, BK, Cheng, VY, Slomka, PJ, Berman, DS, and Dey, D, "Interscan reproducibility of computer-aided epicardial and thoracic fat measurement from noncontrast cardiac CT," J Cardiovasc. Comput Tomogr. 5(3): 172-179 (2011).
[12]Bandekar, AN, Naghavi, M., and Kakadiaris, IA, "Automated pericardial fat quantification in CT data," Conf. Proc. IEEE Eng. Med. Biol. Soc. 1: 932-935 (2006).
[13]Barbosa, JG, Figueiredo, B, Bettencourt, N, and Tavares, JM, "Towards automatic quantification of the epicardial fat in non-contrasted CT images," Comput. Methods Biomech. Biomed. Engin. 14(10): 905-914 (2011).
[14]Udupa, JK, Odhner, D, Zhao, L, Tong, Y, Matsumoto, MM, Ciesielski, KC, Falcao, AX, Vaideeswaran, P, Ciesielski, V, Saboury, B, Mohammadianrasanani, S, Sin, S, Arens, R, Torigian, DA, "Body-wide hierarchical fuzzy modeling, recognition, and delineation of anatomy in medical images," Medical image analysis. 18(5):752-71 (2014).
[15]Wang, HQ, Udupa, JK, Odhner, D, Tong, YB, Zhao, LM, Torigian AD, "Automatic Anatomy Recognition in Whole-Body PET/CT Images," Medical Physics. 43(1): 613-629 (2016).